Derivation of Spatiotemporal Risk Areas and Travel Behaviors During Pandemic Through Reverse Estimation of Mobility Patterns by Agent-Based Modeling

Moongi Choi [a], Alexander Hohl [a]*

[a]*Department of Geography, The University of Utah, Salt Lake City, UT, USA*

*alexander.hohl@geog.utah.edu

Abstract

In response to pandemics, including COVID-19, a significant focus has been placed on proactive response research, such as the prediction of disease cases or identifying risk areas for disease exposure. However, the scarcity of detailed travel data and methodological constraints in predicting past and future individual travel patterns have posed significant challenges. To overcome these challenges, this study introduces an Agent-Based Travel Scheduler (ABTS) model, designed to simulate individual travel patterns. By leveraging limited aggregated travel data sources, which merely track the volume of travels between origins and destinations, the model is capable of decomposing and forecasting travel behaviors into detailed segments, categorized by age, day type, and trip purposes. Through this model, we have explored variations in travel behaviors across past pandemic periods and demographic groups, uncovering complex movement patterns that are closely linked with infection risks. Additionally, we have demonstrated how different age groups adapt their travel in response to the pandemic, offering future insights into targeted disease control strategies for potential future pandemics. By pinpointing travel patterns that have been associated with past pandemic events, it facilitates the formulation of effective proactive responses to potential future pandemics, thereby guiding policy decisions aimed at curbing the spread of infectious diseases.

Keywords: Agent-Based Modeling, Activity-Based Modeling, COVID-19, Activity scheduling, Travel demand

1. Introduction

Since December 2019, the world has faced an unprecedented public health crisis with the outbreak of the COVID-19 pandemic. Although the World Health Organization (WHO) declared the end of the global health emergency in May 2023, several variants of the SARS-CoV-2 still linger (WHO, 2024). Navigating through various mutations and infection waves of the pandemic has altered many aspects of our daily lives, such as travel behaviors (Chauhan et al. 2021; CDC 2024). In response, various fields, including GIScience, have leveraged a range of direct and indirect geographical data in spatial-temporal analyses to strategize resource allocation and prompt responses, aiming to curb future infections. Notably, geospatial dashboards have been extensively utilized for monitoring the geographic spread of the disease (Bernasconi and Grandi 2021; Jo et al. 2022; Hu et al. 2023) and space-time scan statistics for surveillance of disease outbreaks and surges (Desjardins et al. 2018; 2020; Owusu et al. 2019; Hohl et al. 2020).

While these tools effectively represented reactive and active responses by leveraging continuously updated COVID-19 case data (Gupte et al. 2022; Brainard et al. 2023), challenges emerged with proactive responses, such as predicting cases. Key challenges, including untimely updates, insufficient quality, and low spatial-temporal resolution of the data, have significantly impeded model construction (Kogan et al. 2021). These limitations introduced difficulties in developing models aimed at offering preventative solutions, such as predicting the trajectories of infections or identifying exposure risk areas in advance. To effectively implement such strategies, it is crucial to estimate spatial-temporal patterns of exposure by tracking people's travels prior to disease outbreaks. However, this is challenging due to the following:

Firstly, public COVID-19 case data, primarily collected based on patient home address or test center (CDC 2023), leads to a spatiotemporal discrepancy, making it highly challenging to pinpoint the actual areas where infection exposure occurred. Secondly, while past travel data can be used to estimate areas at risk of infection, fine-scale data (e.g., census block group level) is costly and challenging to access. Even when available, this data typically omits crucial demographic details such as gender and

age due to geoprivacy concerns, thereby impeding detailed predictions and the development of targeted containment strategies.

To address these challenges, surveys collecting visitation data from infected individuals have been conducted (Kan et al. 2021). However, the difficulties of continuous data collection and privacy concerns have made it challenging to apply this method in different contexts. Also, studies have simulated travel to identify infection risk areas in urban space (e.g., Mao and Bian, 2010; Zhou et al., 2021). Although their models have been temporally validated, the spatial accuracy of the predicted visit areas has not been similarly validated. While mathematical models like Susceptible-Exposed-Infected-Recovered (SEIR) are used, the inclusion of detailed patterns of travel in estimating spatial contact rates is often overlooked, with the focus primarily on predicting temporal case counts (e.g., Cui et al. 2020; Liu et al. 2020; Feng et al. 2021). Moreover, studies have explored the association between mobility and the spatiotemporal distribution of COVID-19 using smart device data combined with case data (e.g., Badr et al. 2020; Jia et al. 2020), but the transmission trajectories based on individual attributes remain elusive.

This study aims to estimate infection exposure risk areas during the past COVID-19 pandemic through reverse estimation of individual spatiotemporal travel patterns, assisting in formulating effective proactive epidemic strategies for the future. To do this, we developed a simulation model that estimates where individuals visited during the period when a significant number of cases occurred, ultimately giving a solution to bridge the spatiotemporal gap between case report locations and exposure areas. With the data where merely record the sum of travel counts, we decomposed those travels by various criteria, such as age, weekdays/weekends, and trip purpose, to identify more detailed and micro-level past travel patterns. The result of this study reveals who traveled where, for what purpose, and which areas, which could serve as crucial reference data to form targeted disease control strategies for potential future pandemics.

2. Study area, time period and data description

Figure 1 illustrates the pattern of COVID-19 cases in the Milwaukee area, showing two periods of great surges in November 2020 and December 2021 to January 2022 (Wisconsin Department of Health Service, 2023). To reversely estimate the corresponding travel patterns for each surge, the study periods were selected as September to November 2020 (1st period) and October to December 2021 (2nd period). The study area focuses on census tract 55079186300 in Milwaukee, which was among the top 10 of highest Covid-19 cases during both periods, and its surrounding 29 census tracts (encompassing 56 census block groups: CBGs) as shown in Figure 2. The simulation of trips originating from each CBG in the specified study area was conducted to validate the model and interpret the results.

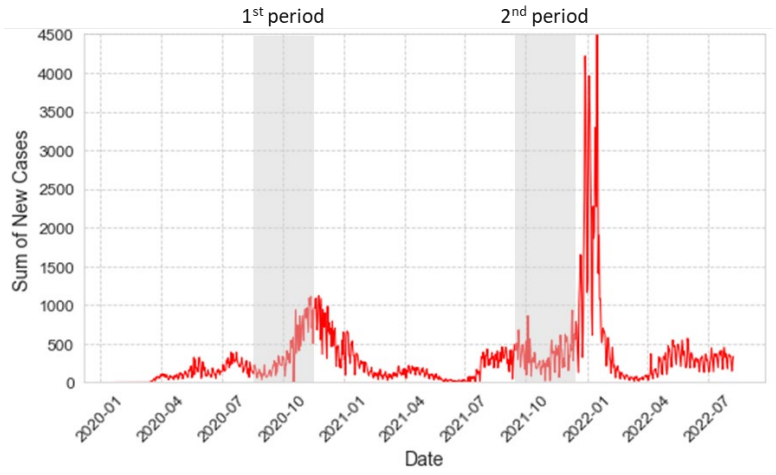

Figure 1. COVID-19 cases in Milwaukee over time

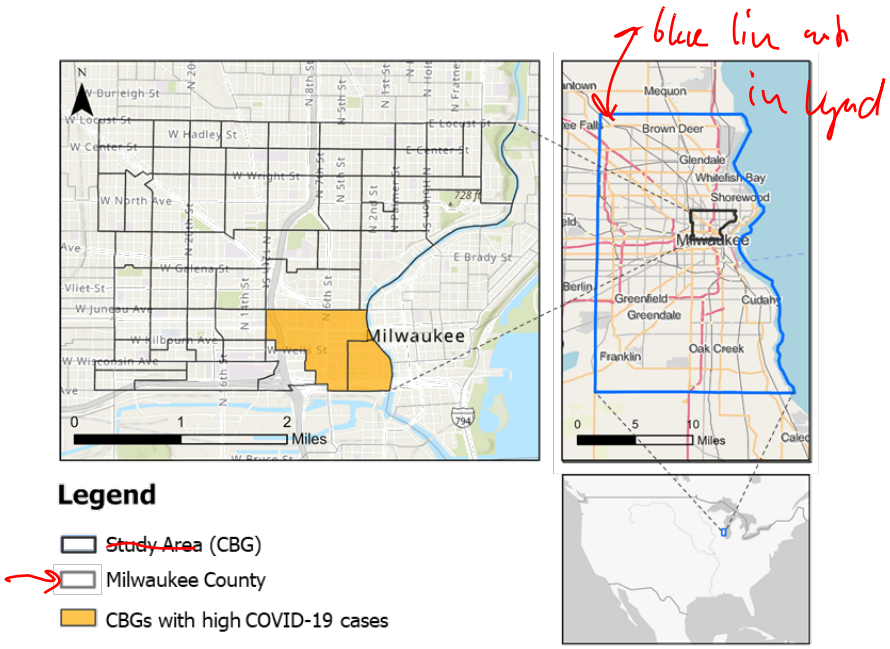

Figure 2. Study area

In this study, we utilized 4 main datasets (Table 1) to establish the ABTS and interpret the results. The Covid-19 case count data was sourced from the Public Health Indicator-Based Information System (IBIS), aggregated by age groups in 10-year intervals and at the census tract level. We utilized this data to identify the periods of elevated COVID-19 risk for each age group and interpreted corresponding travel simulation results.

The National Household Travel Survey (NHTS) is a dataset encompassing detailed information on individual travel patterns across the United States, including trip purpose (e.g., home, work), time, and mode of transportation (e.g., car, bicycle). For our model, we utilized the 2017 NHTS data collected from 197,920 people within Wisconsin to estimate initial/non-calibrated travel schedules in Milwaukee, incorporating probabilistic choices of trip purpose, chain, and mode.

Next, Milwaukee parcel data is a detailed, parcel-level spatial dataset that includes land-use information such as residential, commercial, and agricultural areas. Provided by the Milwaukee County

Land Information Office (MCLIO), we utilized the 2021 dataset to determine the destinations chosen by people for various trip purposes, corresponding to the time period of our study.

The Neighborhood Patterns dataset is a monthly aggregated dataset of mobility, based on individual mobile devices and provided by SafeGraph. This dataset is organized to show the number of people moving in and out of areas at the Census Block Group (CBG) level, either on a random week or as a monthly average. We utilized this data to infer initial individual destination choices at the CBG level and to validate the simulated travel schedules. Additionally, we used the 2021 CBG shapefile data provided by the U.S. Census Bureau to calculate trip distances.

Table 1. Data description

Data	Temporal scale	Spatial scale	Source
Covid-19 cases by age group	Daily (9-11/2020 to 10-12/2021)	Census tract	IBIS
National Household Travel Survey	2017	County	FHWA
Milwaukee parcels	3/2021 updated	Parcel	MCLIO
Neighborhood patterns	Monthly (9~11/2020 to 10~12/2021)	CBG	SafeGraph

3. Concept and framework of Agent-Based Travel Scheduler (ABTS)

Over the past decade, many studies have attempted to incorporate agent-based models with activity-based frameworks (e.g., Bellemans et al., 2010; Gao et al., 2010; Hao et al., 2010, Briem et al., 2019) to generate detailed individual travel patterns from a temporal perspective (Bekhor et al., 2011; Dobler et al., 2014). For instance, in FEATHERS (Janssens et al. 2007; Baqueri et al. 2019), POLARIS (Auld et al. 2016), and MATSim (Axhausen et al. 2016), agent-based microsimulation (e.g., Miller 2019) have been employed to predict individual travel decisions using the characteristics and attributes of each individual as inputs to the scheduler module. This approach allows for the simulation of travel demand and traffic flow based on the independent and autonomous behavior of agents and their

interactions. Therefore, it enables sensitive prediction of mobility changes according to various policy scenarios. Since travel is represented by individual agent behaviors, this approach offers the advantage of facilitating the interpretation of mobility at the micro-scale. In this study, while applying this approach, we aimed to create a flexible and verifiable travel prediction model by developing some parameters that influence individual travels and calibrating them based on real travel data to adapt to diverse spatial environments.

ABTS utilizes a three-step process to generate the initial outcome of individual travel schedules: 1) Comprehensive Travel Classifier, 2) Land-Use Estimator, and 3) Individual Travel Schedule Generator as shown in Figure 3. The output of ABTS includes individual daily trip chains that consists of each trip purpose, occurrence time, destination, duration, and mode, tailored according to age group. Next, a parameter calibration process is undertaken to determine optimized parameters, which are essential for the comparison and validation against observed travel patterns. This process ultimately leads to the generation of the optimal predicted travel schedules.

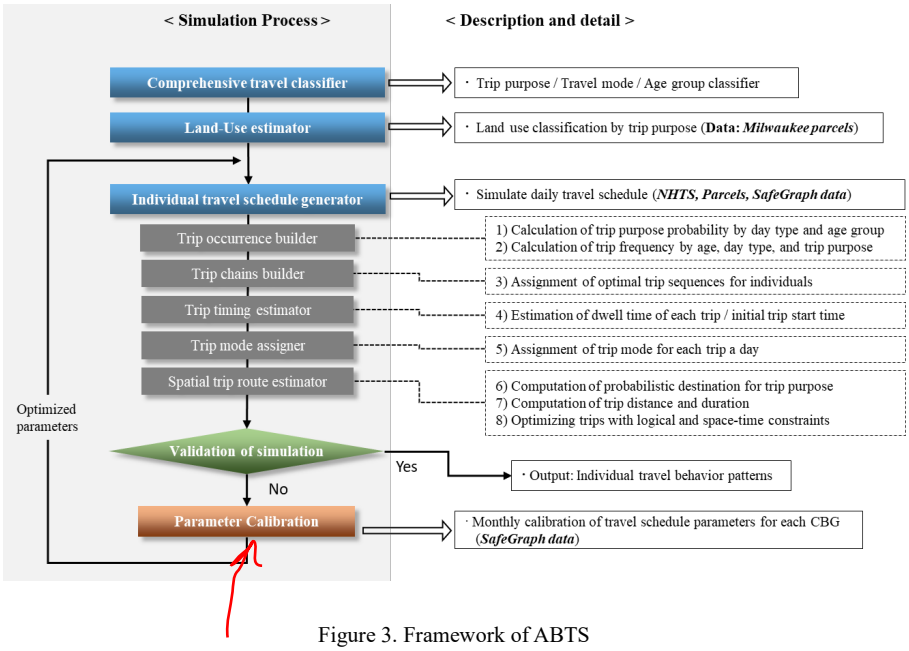

Figure 3. Framework of ABTS

Do you really need color and shadows here?

3.1. Comprehensive travel classifier

Comprehensive travel classifier initially classified trip purposes into nine categories, expanding to thirteen to account for specific activities like School/Daycare/Religious and differentiating between large shopping malls and daily groceries, adapting to land use classifications as shown in Table 2. This nuanced approach builds on previous methodologies, which have varied from four categories (Home, Work, School, Other) as seen in Bowman and Ben-Akiva (2021), to more elaborate classifications up to eleven categories (Arentze and Timmermans, 2004; Labee et al., 2022), offering a tailored classification for predictive modeling.

Trip modes are simplified into four main categories based on NHTS data aggregation. In this study, to facilitate the analysis of the relationship between Covid-19 cases and travel, we excluded outliers such as long trips, and consequently, airplanes were omitted from the trip modes. Lastly, we aligned the age classification with the Covid-19 case data's age groups, dividing it into ten-year intervals and classifying it into five stages: child, teen, adult, mid-adult, and seniors.

Table 2. Classification method in ABTS

Trip purpose (Major)	Trip purpose (Sub)	Trip mode	Age group (range)
1. Home 2. Work 3. School/Daycare/Religious activity (SDR) 4. Daily shopping 5. Buy meals 6. Visiting friends or relatives 7. Recreation/Leisure 8. Service-related trips 9. Others	1. Home 2. Work 3. School 4. University and College 5. Daycare 6. Religious activity 7. Large shopping mall 8. Daily grocery 9. Buy meals 10. Visiting friends or relatives 11. Recreation/Leisure 12. Service-related trips 13. Others	1. Walk 2. Bicycle 3. Car/Motorcycle 4. Public transportation	1. Child (-10) 2. Teen (10-19) 3. Adult (20-39) 4. Mid-Adult (40-59) 5. Seniors (60+)

3.2. Land use estimator

The Land Use Estimator in our study classifies land use attributes to match trip purposes, using parcel data from the Milwaukee area provided by MCLIO. This data includes types such as

residential, school, commercial, and manufacturing, which partially match our trip purposes. To incorporate more specific categories such as daycare, meals, and markets, we used the Google Places API to geocode addresses in Milwaukee related to these purposes. This additional data was then spatially integrated with the parcel data, resulting in thirteen detailed land use categories.

3.3. Individual travel schedule generator

3.3.1. Trip occurrence builder

In the trip occurrence builder, we compute the probability and total number of individual trip occurrences using NHTS data. Equation 1 represents the daily occurrence probability of a trip $P(\theta)$ for each day type d, age group a, and trip purpose t for an individual, using a Naïve Bayes probability model. The day types are categorized into weekdays and weekends, and W_t is a parameter adjusting the occurrence probability for each trip purpose. Here, we denote t and d as superscripts for $W_t^{(t,d)}$ since we can assign different values to it based on the *t* and the *d*.

$$P(\theta_t|X_{a,d}) = \frac{P(X_{a,d}|\theta_t)\cdot W_t^{(t,d)}\cdot P(\theta_t)}{P(X_{a,d})} \quad (1)$$

Subsequently, through these probabilities, the total number of trips k for each agent i is calculated as $k_{t,i} = k_{t,i} \sim multinomial(W_k \cdot \theta_i, [W_t \cdot P_{1,a,d}, W_t \cdot P_{2,a,d}, \dots, W_t \cdot P_{T,a,d}])$. Here, W_k is a parameter that adjusts each individual's daily trip count. $k_{t,i}$ follows a multinomial distribution, where this distribution is sampled for each trip purpose t according to the probability distribution $W_t \cdot p_{1,a,d}$ conditioned on age group, day type, and trip purpose. Additionally, the sum of all daily trip counts $k_{t,i}$ is set to equal θ_i to maintain consistency with the actual data.

3.3.2. Trip chains builder

The Trip Chains Builder follows a three-step process. Firstly, the most similar trip chain O_i

from the NHTS data is selected, based on the number of trips by trip purposes, with the highest similarity score determined by the Kronecker delta function. This function assigns a score of 1 for each matching trip purpose and 0 otherwise, with the total score indicating the level of similarity.

The second step involves setting the first and last trips of S_i to 'Home' and randomly shuffling the remaining trips to form a trip chain. The final step adjusts the trip sequence of S_i to align with the high-similarity trip chain O_i, as per Equation 2. In this process, l serves as an index traversing each trip order in O_i, starting from the first position and incrementally moving to the last. It first checks if the next trip sequence in $O_{i,a,d,l}$ ($O_{i,a,d,l+1}$) exists in $S_{i,a,d}$. If not, it finds the index j where the trip purpose in $S_{i,a,d}$ matches $O_{i,a,d,l+1}$ and then reallocates the corresponding trip purpose in $S_{i,a,d}$ to $O_{i,a,d,l+1}$, effectively rearranging $S_{i,a,d}$.

$$\begin{aligned} &\forall l = 1\ to\ len(O_{i,a,d}): \\ &if\ O_{i,a,d,l+1} \notin S_{i,a,d}, then\ \exists j\ \ where\ S_{i,a,d,j} = O_{i,a,d,l+1} \\ &Then, S_{i,a,d,j} = O_{i,a,d,l+1} \end{aligned} \tag{2}$$

3.3.3. Trip timing estimator

The trip timing estimator calculates each trip's dwell time and the initial start time from home. Dwell time is derived by sampling from NHTS data, considering factors like age group (a), day type (d), trip purpose (t), and daily trip count (k). This process acknowledges patterns such as teenagers' shorter dwell times for work due to part-time jobs and the trend of shorter dwell times with higher daily trip counts for the same purpose. Here, trip counts are categorized into 1 trip (62,984 individuals), 2-3 trips (66,126 individuals), and 4+ trips (68,810 individuals) per day.

We then create dwell time probability distributions based on a, d, k' (categorized k), and t, sampling from these to assign dwell times (DT_i^t) for each individual's trip. The initial trip start time is similarly estimated by sampling from a distribution based on age group, day type, and trip purpose.

3.3.4. Trip mode assigner

In assigning individual's trip modes, we utilize NHTS data for sampling, while adopting heuristic approaches to establish rules. The procedure is as follows: Firstly, if an individual i has no trips outside planned, no trip mode is assigned. Otherwise, for each individual i, trip modes for their k^{th} trips are initially assigned by sampling from a probability distribution. This distribution is tailored based on the individual's age and the purpose of each trip.

Subsequently, defined conditions are applied to individuals whose first trip mode is 'Car'. The first condition is that the last trip mode must be 'Car', which is based on the logical inference that if one departs in a personal vehicle, they should return in it. We excluded outliers such as taxi usage, focusing solely on personal vehicle usage. The second condition pertains to non-round trips, where a change in trip mode implies the inability to retrieve a car left at a previous location, necessitating all subsequent trip modes to be 'Car'.

3.3.5. Spatial trip route estimator

In the Spatial Trip Route Estimator, destinations for each trip purpose (CBG level) are determined based on the interaction between distance, land use, and the agents' choices. Subsequently, through logical and space-time constraints, an optimal final schedule for each individual is generated.

Equation 3 is utilized to probabilistically determine the destination D for each trip purpose. The initial probabilities are computed based on observed monthly records of destination choices from the origin area A, derived from SafeGraph data. Since this study involves reverse estimation of past travel, observed travel data can be used to establish initial destination choices. However, for predictions without previous travel data, this probability can be set to 1 that is only affected by other parameters.

Since the SafeGraph data is not categorized by trip purpose but solely aggregated as counts, two formulas are multiplied to calculate the probability for each trip purpose-specific destination. The first formula is the probability based on the count of places related to trip purpose t, denoted as $C^{(t)}$,

this is important and sets your work apart from SafeGraph

obtained from land use data. This probability increases if there are more places related to the trip purpose in the land use, and its weight is designated as W_s, named 'spatial attractiveness weight'. The second is a distance sensitivity formula based on the distance decay function. A higher weight W_d indicates that the distance $d(A, D)$ between the origin and the destination significantly influences the choice of destination, whereas a lower weight implies that distance is not a major factor.

$$P_t(A \to D) = \frac{k_{A \to D}}{k_A} \times \left(\frac{C^{(t)}(D)}{\sum_j C^{(t)}(D_j)} \right)^{W_s^{(t)}} \times e^{-W_d^{(t)} \cdot d(A,D)} \quad (3)$$

Commented [MC1]: Where밑을 지웠음. 글고 normalization을 없앴음.
설명들이 where을 지워도 되는지, normalization을 없애도 되는지 파악

Once the trip destination for each trip purpose is assigned, trip distances and durations are estimated using OpenStreetMap (OSM) data via the OSMnx Python library. Given the high computational demands of calculating network distances for all trips, a sampling approach was adopted. In Milwaukee, random points across Census Block Groups (CBGs) were selected to calculate the ratio of network road distance to straight-line distance, resulting in a factor of 1.223. Thus, a straight-line distance of 10 miles translates to an estimated trip distance of 12.23 miles.

To compute the trip duration of each trip, speed settings for different trip modes were based on the study by Alves et al. (2020). Walking speeds varied by age group (child, teen: 4.82 km/h; adult: 4.54–4.82 km/h; mid-adult: 4.43–4.54 km/h; seniors: 3.42–4.34 km/h). The average speeds for cars, public transportation, and bicycles were derived from Milwaukee's NHTS subset data, recorded as 39.74 km/h, 18.79 km/h, and 7.72 km/h, respectively.

To estimate optimal travel schedules, three main constraints were applied: limiting the study to the Milwaukee area to focus on internal mobility and COVID-19 exposure; adjusting unrealistic trips, such as converting walking trips over an hour to public transportation; and modifying schedules that result in excessively long trips or an unreasonable number of trips, especially those ending between 2 a.m. and 6 a.m.

4. Model validation

For the calibration of the simulation, the parameters W_k, W_t, W_s, and W_d were employed, each set to unique values for the 56 CBGs in the study area. Calibration was employed monthly neighborhood data. This involved comparing the simulated total trip count for one week per month with the observed data to evaluate W_k, and calibrating the remaining parameters by comparing the simulated spatial travel flows with the observed data for each month. Population settings for each age group within each CBG, utilized in multiple simulation runs, were sourced from the American Community Survey (ACS) data provided by the Census.

Initially, for the monthly optimal parameter values of W_k, we generated travel schedules 100 times for each month in every CBG, resulting in a total of 33,600 runs ($56\ CBGs \times 6\ months \times 100\ runs$). We then compared the average total trip counts from these schedules with the observed trip counts. The model accuracy of this trip count comparison was calculated by: $Simulated\ Trip\ Counts\ /\ Observed\ Trip\ Counts \times 100$.

Next, we calibrated the optimal parameter values for W_t, W_s, and W_d. To calibrate W_t, we selected the four most frequent trip purposes identified in the Milwaukee area's NHTS data: Daily Shopping, School/Daycare/Religious Activities (SDR), Work, and Buy Meals. Although the trip weights W_t are already data-informed, being derived from the trip occurrence probabilities in the existing NHTS data, further calibration of the parameters most influential on the number of trips can mitigate excessive computational intensity while improving predictive overall accuracy of the model. For each of these trip purposes, specific parameter ranges were defined (W_t: 0.5 to 1.25 with increments of 0.25; W_s: 0 to 1.5 with increments of 0.5; W_d: 0 to 0.75 with increments of 0.25).

We randomly set parameters and conducted approximately 1,000 trials for each CBG with 20% of population each month, resulting in a total of 336,000 runs ($56\ CBG \times 6\ month \times 1{,}000\ runs$). Subsequently, a Machine Learning (ML) based surrogate model was employed to carry out the calibration for each CBG. The surrogate model technique is often used in simulation studies when

excessive computational intensity is required for sensitivity analysis or calibration due to extensive parameter spaces (Arbab et al., 2016; Ligmann-Zielinska et al., 2020; Chen et al., 2021).

For the method, we utilized Random Forest (RF) predictions, known for better accuracy in modeling nonlinear relationships. We set the hyperparameters 'n_estimators' (100, 200, 300, 400, 500) and 'max_depth' (3, 5, 7, 9), and employed 5-fold cross-validation to select the model with the highest model accuracy, as described in Equation 4. The accuracy assessment involved min-max normalization of all unique trips n from a single CBG to each destination, comparing the simulated number of trips $\hat{s}_i$ with observed trips $\hat{o}_i$. As a final step for prediction, we conducted 100 simulations for each CBG using the actual population data and the optimal parameter combination with the highest accuracy from the RF model.

$$ModelAccuracy_{CBG} = \frac{1}{n}\sum_{i=1}^{n}(1 - |\hat{s}_i - \hat{o}_i|) \quad (4)$$

5. Results

5.1. Interpretation of monthly travel patterns through calibration results

The monthly calibrated results of W_k are presented in Table 3. Most results showed over 98% accuracy, indicating that the simulation predicts total trip counts very effectively. Observing the variations in trip counts through W_k, a significant reduction in trip counts was noted in November 2020 in weekdays, coinciding with the onset of the COVID-19 peak as shown in Figure 1. Next, the trip counts in October, November, and December of 2021 mirrored those of November 2020. A slight increase was observed in November 2021 compared to October, but December continued to show low trip counts.

Table 3. Calibration results of W_k

Date	Week	W_k	Total trip count		Model accuracy
			Simulated	Observed	
2020 09	Weekday	0.39	61112.6	61091.16	99.965
	Weekend	0.5	21943.64	21316.56	97.142

2020 10	Weekday	0.39	61112.6	62211.92	98.233
	Weekend	0.52	22045.6	22173.04	99.425
2020 11	Weekday	0.34	55122.56	53847.36	97.687
	Weekend	0.64	26457.16	26460.2	99.989
2021 10	Weekday	0.34	56394.4	55038.72	97.596
	Weekend	0.66	26061.09	26549.84	98.159
2021 11	Weekday	0.37	58861.96	58043.64	98.61
	Weekend	0.54	21727.61	21991.52	98.8
2021 12	Weekday	0.34	56394.4	54385.24	96.437
	Weekend	0.48	19905.25	19815.48	99.549

Figure 4 presents the monthly averaged results of the calibrated W_t. W_t serves as a weight adjusting the occurrence probability of each trip, with higher values indicating a higher number of trips for that purpose. The results reveal that during the first COVID-19 surge (2020. 09 ~ 11), there was a decline in weekday work-related trips. However, following October 2021, which marks the second surge, there was an overall increase. In contrast, trips for buying meals, daily shopping, and School/Daycare/Religious activities (SDR) were higher during the first surge and decreased in the second. Notably, daily shopping and SDR showed higher values on weekends compared to weekdays, while trips for meals were almost equal on weekdays and weekends. Work-related trips were more prevalent on weekdays.

These patterns imply that the first wave of COVID-19 infections seems to have arisen from a combination of exposures across diverse locations, including workplaces, shopping, religious or school gatherings, and meal settings, whereas the second wave appears to be predominantly driven by exposures in workplace environments. A more detailed examination of these travel trends, particularly focusing on differences by age, will be described in Section 5.2.

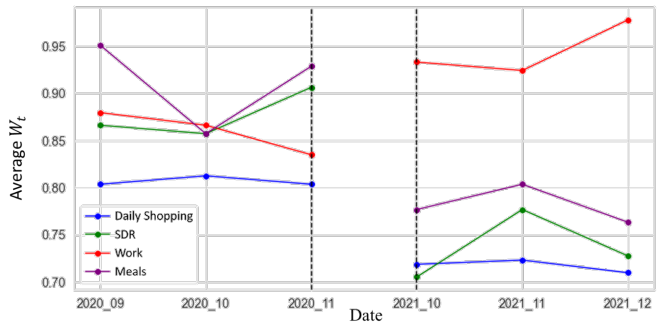

(a)

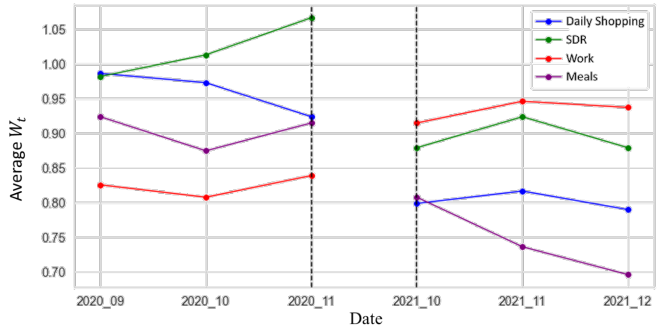

(b)

Figure 4. Calibration results of W_t (a: weekday, b: weekend)

Table 4 presents the average monthly calibrated results of W_s and W_d across all CBGs. W_s, representing the spatial attractiveness weight, was consistently highest for Work trips throughout the period, followed by Meals, SDR, and Daily Shopping. This indicates that most people in Milwaukee commute to CBGs with a high concentration of workplaces. Between 2020 and 2021, the variation in W_s for trip purposes such as SDR, work, and meals showed minimal differences, while daily shopping trips exhibited a notable variation. This suggests that during the initial COVID-19 outbreak in 2020, there was a pronounced preference for shopping at large supermarkets or markets-rich areas, a trend that diminished in 2021, reflecting a reduction in stockpiling behavior during the pandemic's later stages.

As for W_d, the distance sensitivity weight, Work also had the highest value. This implies that

trips to workplaces are greatly influenced by distance, indicating a preference for commuting to workplaces closer to home. Also, the lack of significant change in W_d across different trip purposes between 2020 and 2021 suggests that COVID-19 had minimal impact on the distance factor in destination choices.

Table 4. Calibration results of W_s and W_d

Date	W_s				W_d				RMSE	Model Accuracy	Validation Accuracy (WD/WK)
	D_shop	SDR	Work	Meals	D_shop	SDR	Work	Meals			
2020 09	0.161	0.25	0.786	0.464	0.375	0.451	0.509	0.406	0.01	0.854	0.83/0.768
2020 10	0.33	0.214	0.616	0.348	0.429	0.388	0.589	0.286	0.01	0.861	0.831/0.754
2020 11	0.241	0.196	0.804	0.455	0.415	0.348	0.491	0.379	0.009	0.833	0.792/0.711
2021 10	0.089	0.232	0.67	0.41	0.46	0.504	0.571	0.402	0.006	0.852	0.841/0.839
2021 11	0.018	0.25	0.86	0.286	0.393	0.362	0.616	0.388	0.007	0.864	0.843/0.83
2021 12	0.063	0.33	0.669	0.205	0.491	0.48	0.558	0.259	0.008	0.848	0.835/0.824
Average	0.15	0.245	0.734	0.361	0.427	0.422	0.556	0.353	0.008	0.84	0.829/0.788

* WD: Weekday, WK: weekend

The RF model used for calibrating W_t, W_s, and W_d exhibited an average accuracy of 0.84 and a RMSE of 0.008 over the entire period. Subsequent validation using the final selected optimal parameter combination demonstrated approximately 80% accuracy for both weekdays and weekends. Figure 5 presents a graph of the residuals throughout the entire study period. The residuals were on average 102.28, with a standard deviation of 1,370, and quartile values at 25%: 55.483, 50%: 186.20, and 75%: 368. This close distribution around 0 and random dispersion suggests that the model effectively predicts travel patterns and is unbiased.

However, September and October 2020 resulted in outlier residuals for CBG 550790144001, with actual visits (91,433 in September and 89,494 in October) far exceeding model predictions, by nearly 70,000 more than any other CBG. This discrepancy, with residuals of 77,482 in September and 72,656 in October, despite predicted counts of 13,951.1 and 16,838.4, respectively, suggests extraordinary activity in this area, possibly due to its city square, city hall, hotels, and health care centers being used as vaccination or quarantine sites. This indicates the model's limitations in capturing such

anomalies.

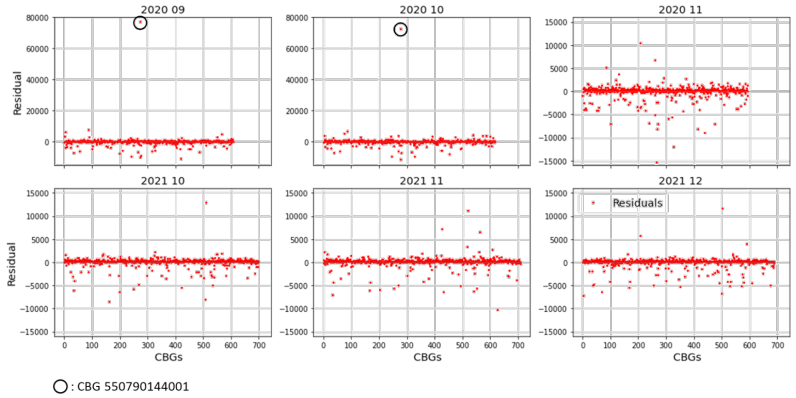

Figure 5. Residual patterns across the study period

Further analysis using Moran's I test for spatial autocorrelation, with a contiguity-based conceptualization, yielded a Moran's index of 0.0165 and a p-value of 0.274. This indicates a very weak, non-significant spatial correlation, suggesting the model's travel pattern predictions are not spatially biased. However, the residual map highlighted a tendency for the model to overpredict movements within CBGs in study area as shown in Figure 6, pointing to inaccuracies in simulating intra-CBG travel.

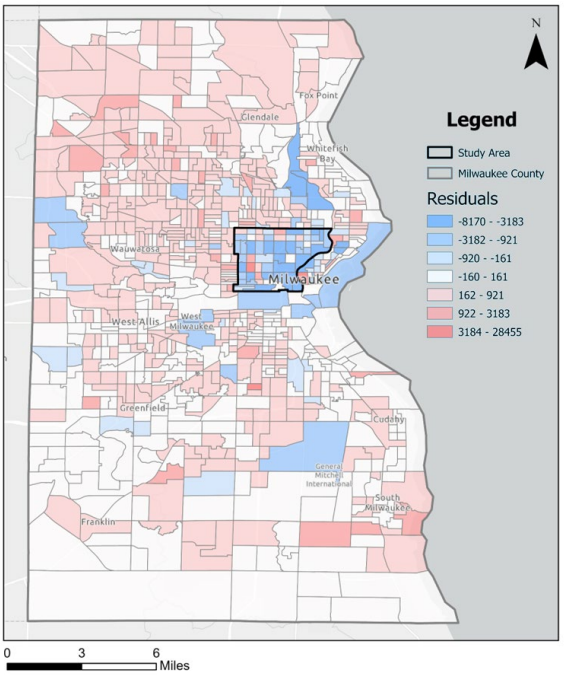

Figure 6. Spatial distribution of residual across CBGs

5.2. Simulated past travels

5.2.1. Tracing temporal travel behavior trends

The cumulative age-specific COVID-19 cases in Wisconsin over time are presented, showing a gradual increase in infections across all age groups in both periods, following the order of adult, mid-adult, teen, seniors, and child, as shown in Figure 7. Notably, in the first period (a), Adults exhibited a rapid increase in cases starting in mid-October, while in the second period (b), a sharp rise was observed after mid-December.

Figure 8 displays the average number of top 3 trip purposes per age group, weekday/weekend, in both periods, providing an estimation of the travel patterns potentially most associated with external

infection for each age group by time. Weekdays are represented by straight lines, whereas weekends are represented by dotted lines.

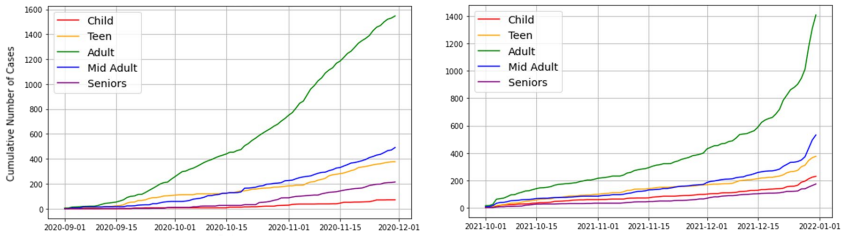

Figure 7. Cumulative Covid-19 cases by age group (a: 1st period, b: 2nd period)

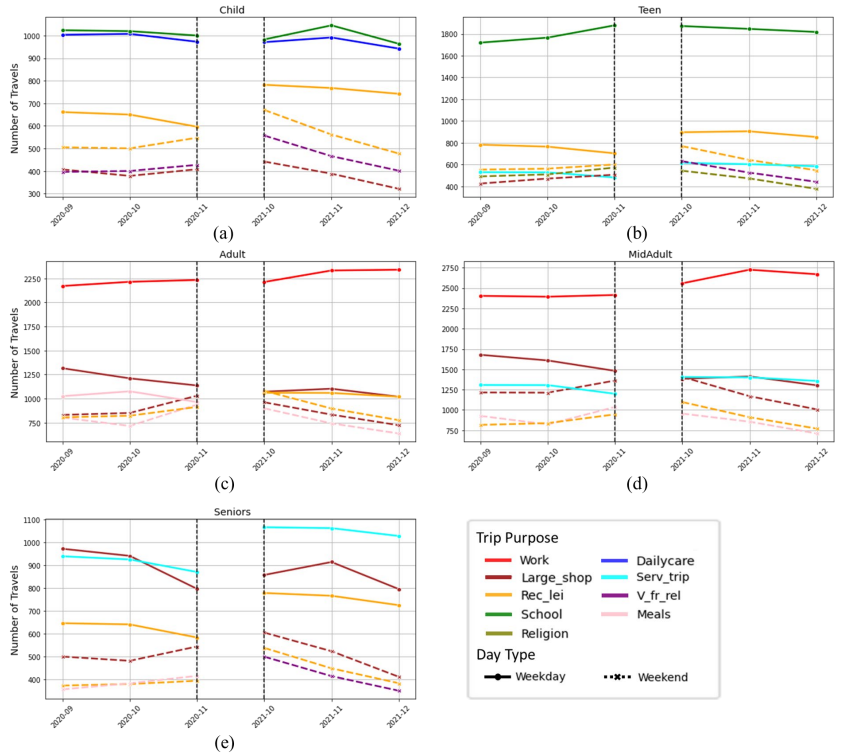

Figure 8. Top 3 travels by day type over time for age groups
(a: child, b: teen, c: adult, d: mid-adult, e: seniors)

italicize

Initially, for child group in both the first and second periods, the most frequent travels during weekdays were to school, daily care, and recreation and leisure (rec_lei) trips. During weekends, the sequence was rec_lei, visiting friends or relatives (v_fr_rel), and large shopping malls (large_shop). It suggests that infections in children likely occurred during trips to school and daily care on weekdays, and rec_lei and v_fr_rel on weekends, without a specific change in travel patterns.

For teen group, in both periods, school trips were the most frequent on weekdays, followed by rec_lei and service-related trips (serv_trip). Serv_trip could involve library visits, museums, volunteer facilities, and internship agencies for school projects, assignments, volunteer activities, and career exploration. Trips for v_fr_rel ranked fourth. On weekends, rec_lei and religious activities (religion) were predominant, with a shift towards more v_fr_rel trips in the second period, suggesting a reduced precaution of infection risk from social interaction.

For adults, work-related trips were overwhelmingly the most frequent on weekdays in both periods, with the first period's second and third most frequent trips being large_shop and for meals, and the second period's being large_shop and rec_lei. This indicates that work trips likely contributed significantly to adult COVID-19 infections, especially in the second period when other trips decreased while work trips increased after November 2021. In addition, shopping trips gradually decreased yet remained high. During weekends, large_shop, rec_lei, and meals were the top 3 in both periods, with slight differences.

Mid-adults also prioritized work trips, with an increase observed in the second period, possibly due to reduced teleworking. This might have contributed to the sharp increase in COVID-19 cases among the mid-adult age group in the second period. Following work, large_shop and serv_trip were next most frequent trips in both periods. During weekends, large_shop trips were most frequent, followed by rec_lei and meals.

Lastly, for seniors, during weekdays in the first period, large_shop and serv_trip were the top 2 trip purposes, followed by rec_lei, showing a decreasing trend. Notably, the number of trips increased more in the second period than in the first. During weekends in the first period, large_shop, rec_lei, and

meals were the top 3, while in the second period, large_shop, rec_lei, and v_fr_rel were the top 3. All simulated results of average monthly trips and dwell times per age group, period, day type, and CBG can be found in Tables 6 and 7 in Appendix.

5.2.2. Tracing past exposure risk to COVID-19 in space

To analyze travel patterns during peak COVID-19 periods, we mapped simulated travel counts to various destinations across age groups, as shown in Figure 9. A subset map of the study area highlighted the spatial distribution of COVID-19 cases and travel pattern differences. In the first and second periods, trip counts ranged from 18 to 209,386 and 28 to 166,731, with average trips of 6,728 and 6,103, respectively.

Travel patterns were similar across both periods, though the 2nd period shows a reduction in overall travel. Six destination CBG groups were identified as primary destinations for people from the study area and Table 5 lists the top three trip purposes for these destinations. Areas A and A' featured large shopping centers, parks, and recreational facilities such as soccer and baseball fields, leading to high counts of trips for Large_shop, meals, and Rec_lei. Area B, with its outdoor golf club, sports stadium, and medical complex, resulted in Rec_lei and Serv_trip as most common. Area C, a multifunctional downtown area including a sports arena, museums, and universities, showed a diverse land-use pattern, with significant trips to workplaces, Large_shop and meals.

Area D, along the coast, features tourist spots, parks, stadiums, a hospital complex, and insurance companies, leading to many Rec_lei and Serv_trip visits. Area E, with its mix of supermarkets, grocery stores, auto repair centers, stadiums, and hotels, exhibits frequent Rec_lei, large_shop, and serv_trip visits. Lastly, area F, where Milwaukee International Airport is located, along with parks, hotels, and pharmacies, exhibited a high number of Rec_lei and Serv_trip. V_fr_rel trips were prevalent in many areas, due to the presence of residential areas throughout.

Figure 9. Spatial patterns of Covid-19 cases and travel counts from the study area (a:1st period, b: 2nd period)

Table 5. Trip purposes and counts in each CBG

CBGs	Group	Top 3 trip purpose *(count in thousand)*
550790044001 550790044003 550790602001	A	Large_shop (64), Meals (48), Rec_lei (21)
	A’	Meals (32), Large_shop (19), Rec_lei (19)
550790902002 550790903001 550791853001	B	Rec_lei (14), Serv_trip (12), V_fr_rel (10)
	B’	Rec_lei (16), Serv_trip (14), V_fr_rel (12)

550790141001 550790144001 550790146001 550790146002 550790147002 550791863001 550791863002 550791864001 550791864002	C	Work (182), Large_shop (166), Meals (107)
	C’	Work (165), Large_shop (116), Meals (90)
550799800001	D	Rec_lei (53), Serv_trip (41), V_fr_rel (37)
	D’	Rec_lei (30), Serv_trip (24), V_fr_rel (21)
550791101001 550791101002 550791101003	E	Rec_lei (21), Large_shop (21), Serv_trip (18)
	E’	Rec_lei (17), Serv_trip (15), V_fr_rel (13)
550790216001 550790217005	F	Rec_lei (6), Serv_trip (5), V_fr_rel (4)
	F’	Rec_lei (5), Serv_trip (4), V_fr_rel (4)

Comparing the COVID-19 case maps of the study area (Census tract level) with the trip destination pattern (CBG level) in subset maps in Figure 9 reveals that in areas with high case numbers, the number of trips was also high in some instances. However, there were also cases where trip counts were lower than expected in high-case areas, and vice versa. This discrepancy underscores the importance of considering travel when designing policies to curb disease spread, emphasizing that reliance on COVID-19 record data alone is insufficient and that the spatiotemporal risk of exposure should be assessed by considering travel patterns.

Figure 10 illustrates the travel patterns of specific age groups during the 1st and 2nd periods departing from two CBGs: 550791863001 and 550791863002 (Census tract: 55079186300), which recorded the highest COVID-19 infections in both periods. The population for each age group in these CBGs in 2020 was child: 62, teen: 298, adult: 2323, mid-adult: 1573, seniors: 168, and child: 128, teen: 288, adult: 2270, mid-adult: 1653, seniors: 207 in 2021. Figure 10(a) and (b) show the count of work trips for the adult and mid-adult age groups to destination CBGs. The average trip count values for the 1st and 2nd periods were 1137.1 and 1279.12 respectively, with the 2nd period displaying a slightly more dispersed spatial pattern. Figures 10(c) and (d) depict the number of Rec_lei trips for the child and teen groups in both periods, with averages of 33.26 and 29.37 respectively, indicating that a more

diverse range of locations was visited in the 2nd period compared to the 1st.

This ability to estimate the count and spatial distribution of trips from one area to another by age group and trip purpose offers more detailed and varied insights than what mobile device mobility data can provide. This can make a valuable contribution to predicting pathways of epidemic spread, identifying areas at risk of infection, and formulating effective disease control strategies.

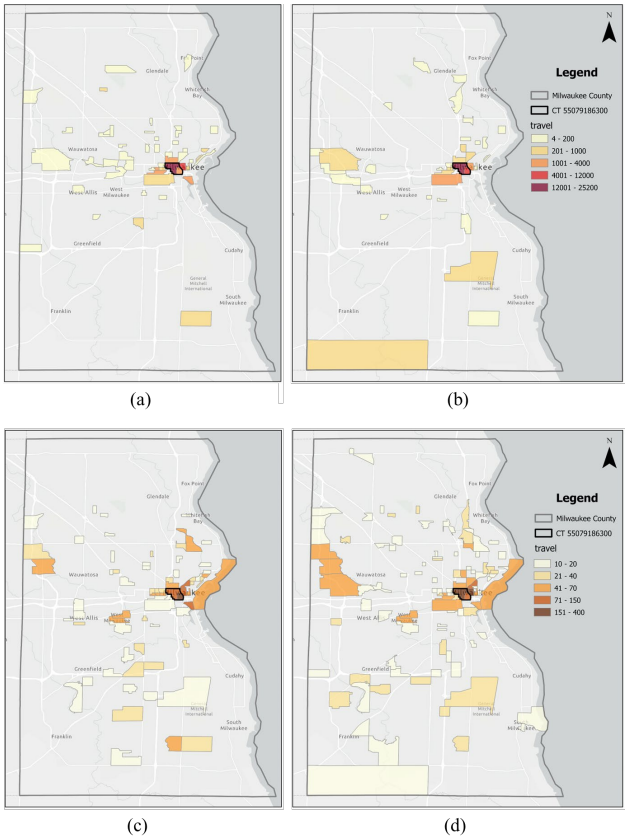

Figure 10. Covid-19 peak area travel patterns (a and b: 1st and 2nd periods – adult/mid-adult at work; c and d: 1st and 2nd periods – child and teen, Rec_lei)

6. Discussion and conclusion

In this study, we aimed to reverse-estimate the areas and travel patterns associated with high risk of infection exposure during the previous COVID-19 pandemic, to develop more sophisticated strategies for prevention and efficient resource allocation for a potential future global pandemic. To achieve this, we proposed the Agent-Based Travel Scheduler (ABTS) model, which is adaptable to various policies and future scenarios through parameter calibration and data replacement for future population and land use.

Firstly, we calibrated the weight parameters (W_k, W_t, W_s, W_d) using aggregated travel data based on smart device locations to examine the comprehensive travel patterns in the Milwaukee area study region. Total trip counts (W_k) decreased as it approached the COVID-19 peak in the latter half of the first period (2020/09 ~ 2020/11) and remained lower in the second period (2021/10 ~ 2021/12). Trip purpose-specific counts (W_t) showed that in the first period, daily shopping, religious or school attendance, meals, and work trips were all similarly high, but in the second period, work trips significantly increased, likely due to a decrease in teleworking. The spatial attractiveness weight (W_s) was highest for work throughout all periods, and shopping was particularly high in the first period. This suggests that people in the Milwaukee study area commute to places with many workplaces, and visits to large supermarkets were frequent during the first period, possibly for stockpiling essentials. The distance sensitivity weight (W_d) was also highest for work trips, indicating a preference for workplaces closer to home.

Secondly, temporal travel behavior trends by age revealed that different age groups have distinct travel patterns, potentially affecting their exposure to infection. For children, school-related activities and daily care were primary during weekdays, whereas recreation and leisure activities were more prominent during weekends. Teenagers mainly traveled to school on weekdays, with recreation, leisure, and service-related trips also being significant. Their weekend travels varied, but leisure activities often ranked high. Adults and mid-adults predominantly traveled for work during weekdays, followed by shopping and meals. Seniors showed increased travel activities in the second period, with

large shopping and service-related trips being most frequent.

Lastly, we interpreted the travel patterns in space during the two periods by investigating which places and trip purposes were related to the COVID-19 case infections in different age groups. The trip purpose of each visit varied by CBG, with trips to nearby places being mainly for work, and trips for shopping, meals, and recreation showing a more spatially dispersed pattern. By displaying these travel patterns at the individual CBG level by age, trip purpose, and period, we identified the potential for using the results to devise effective and granular disease control strategies.

The approach in this study has several advantages. Using historical travel data collected through mobile devices, the ABTS enables reverse-estimation and decomposition of travel patterns by age and trip purpose. This approach facilitates targeted disease prevention strategies. For example, it can identify the periods, routes, and locations where children and teenagers are more likely to be infected, informing more effective resource allocation and enhanced safety measures in educational institutions. The model also has potential for proactive strategies against future pandemics by referring to the estimated spatiotemporal travel behavior and patterns observed during the past COVID-19 pandemic. Additionally, the ABTS model can incorporate future population, land use changes, and changes in travel habits with parameters, making it useful for developing long-term public health plans through various scenarios.

However, this study encounters certain inevitable constraints. The model showed difficulty in accurately predicting trip counts resulting from specific events causing abnormal travel patterns. Therefore, algorithm modifications are needed to reflect such anomalies by strongly weighting spatial attractiveness in specific CBGs affected by events. Additionally, simulated trip counts tended to be higher than observed counts within the study area. Although Morans'I of the residuals was not statistically significant, addressing this issue by penalizing trip counts to starting points (residential area) through algorithm adjustments will be necessary.

Additionally, despite accounting for complex interactions between age, weekdays/weekends, trip purpose probabilities, distance, and land use in the travel predictions, the influence of social

interactions such as with family, friends, and colleagues was not considered. Future research could explore the integration of social media or other alternative social network data into the ABTS model. This could involve applying analytical models such as the DeGroot (1974) model or the Hegselmann-Krause model (Rainer and Krause, 2002), thereby enriching the ABTS with parameters that capture complex social interactions. Adopting other factors influencing trip demand, such as socioeconomic factors, in addition to demographic characteristics like age, could further improve the prediction of travel schedules.

Reference

Arentze, T. A., & Timmermans, H. J. (2004). A learning-based transportation-oriented simulation system. Transportation Research Part B: Methodological, 38(7), 613-633.

Arbab, N. N., Collins, A. R. & Conley, J. F. (2016). Projections of watershed pollutant loads using a spatially explicit, agent-based land use conversion model: A case study of Berkeley County, West Virginia. Applied Spatial Analysis and Policy, (pp. 1–3s)

Auld, J., Hope, M., Ley, H., Sokolov, V., Xu, B., & Zhang, K. (2016). POLARIS: Agent-based modeling framework development and implementation for integrated travel demand and network and operations simulations. Transportation Research Part C: Emerging Technologies, 64, 101-116.

Axhausen, K. W., & Gärling, T. (1992). Activity-based approaches to travel analysis: conceptual frameworks, models, and research problems. Transport reviews, 12(4), 323-341.

Axhausen, K. W., Horni, A., & Nagel, K. (2016). The multi-agent transport simulation MATSim (p. 618). Ubiquity Press.

Badr, H. S., Du, H., Marshall, M., Dong, E., Squire, M. M., & Gardner, L. M. (2020). Association between mobility patterns and COVID-19 transmission in the USA: a mathematical modelling study. The Lancet Infectious Diseases, 20(11), 1247-1254.

Baqueri, S. F. A., Adnan, M., Kochan, B., & Bellemans, T. (2019). Activity-based model for medium-sized cities considering external activity–travel: Enhancing FEATHERS framework. Future Generation Computer Systems, 96, 51-63.

Bekhor, S., C. Dobler and K. W. Axhausen (2011) Integration of activity-based with agent-based models: an example from the Tel Aviv model and MATSim, Transportation Research Record, 2255, 38–47.

Bellemans, T., Kochan, B., Janssens, D., Wets, G., Arentze, T., & Timmermans, H. (2010). Implementation framework and development trajectory of FEATHERS activity-based simulation platform. Transportation Research Record, 2175(1), 111-119.

Bernasconi, A., & Grandi, S. (2021). A conceptual model for geo-online exploratory data visualization: The case of the covid-19 pandemic. Information, 12(2), 69.

Bhat, C. R., & Koppelman, F. S. (1999). Activity-based modeling of travel demand. In Handbook of transportation Science (pp. 35-61). Boston, MA: Springer US.

Bowman, J. L., & Ben-Akiva, M. E. (2001). Activity-based disaggregate travel demand model system with activity schedules. Transportation research part a: policy and practice, 35(1), 1-28.

Brainard, J., Lake, I. R., Morbey, R. A., Jones, N. R., Elliot, A. J., & Hunter, P. R. (2023). Comparison of surveillance systems for monitoring COVID-19 in England: a retrospective observational study. The Lancet Public Health, 8(11), e850-e858.

Briem, L., Mallig, N., & Vortisch, P. (2019). Creating an integrated agent-based travel demand model by combining mobiTopp and MATSim. Procedia Computer Science, 151, 776-781.

Centers for Disease Control and Prevention. (2023). COVID Data Tracker. Retrieved January 25, 2024, from https://covid.cdc.gov/covid-data-tracker/#maps_new-admissions-rate-county

Centers for Disease Control and Prevention. (2024). SARS-COV-2 Variant Classifications and Definitions. Retrieved January 25, 2024, from. https://www.cdc.gov/coronavirus/2019-ncov/variants/variant-classifications.html

Chauhan, R. S., Bhagat-Conway, M. W., Capasso da Silva, D., Salon, D., Shamshiripour, A., Rahimi, E., ... & Pendyala, R. (2021). A database of travel-related behaviors and attitudes before, during, and after COVID-19 in the United States. Scientific Data, 8(1), 245.

Chen, S. H., Londoño-Larrea, P., McGough, A. S., Bible, A. N., Gunaratne, C., Araujo-Granda, P. A., ... & Fuentes-Cabrera, M. (2021). Application of machine learning techniques to an agent-based model of pantoea. Frontiers in Microbiology, 2638.

Cui, Q., Hu, Z., Li, Y., Han, J., Teng, Z., & Qian, J. (2020). Dynamic variations of the COVID-19 disease at different quarantine strategies in Wuhan and mainland China. Journal of infection and public health, 13(6), 849-855.

DeGroot, M. H. (1974). Reaching a consensus. Journal of the American Statistical association, 69(345), 118-121.

Desjardins, M. R., Hohl, A., & Delmelle, E. M. (2020). Rapid surveillance of COVID-19 in the United States using a prospective space-time scan statistic: Detecting and evaluating emerging clusters. Applied geography, 118, 102202.

Desjardins, M. R., Whiteman, A., Casas, I., & Delmelle, E. (2018). Space-time clusters and co-occurrence of chikungunya and dengue fever in Colombia from 2015 to 2016. Acta tropica, 185, 77-85.

Dobler, C., Horni, A., & Axhausen, K. W. (2014). Integration of activity-based and agent-based models: Recent developments for Tel Aviv, Israel. Arbeitsberichte Verkehrs-und Raumplanung, 1027.

Feng, S., Feng, Z., Ling, C., Chang, C., & Feng, Z. (2021). Prediction of the COVID-19 epidemic trends based on SEIR and AI models. PLoS One, 16(1), e0245101.

Gao, W., Balmer, M., & Miller, E. J. (2010). Comparison of MATSim and EMME/2 on greater Toronto and Hamilton area network, Canada. Transportation Research Record, 2197(1), 118-128.

Gupte, V., Hegde, R., Sawant, S., Kalathingal, K., Jadhav, S., Malabade, R., & Gogtay, J. (2022). Safety and clinical outcomes of remdesivir in hospitalised COVID-19 patients: a retrospective analysis of active surveillance database. BMC Infectious Diseases, 22(1), 1.

Hao, J. Y., Hatzopoulou, M., & Miller, E. J. (2010). Integrating an activity-based travel demand model with dynamic traffic assignment and emission models: Implementation in the Greater Toronto, Canada, area. Transportation Research Record, 2176(1), 1-13.

Hohl, A., Delmelle, E. M., Desjardins, M. R., & Lan, Y. (2020). Daily surveillance of COVID-19 using the prospective space-time scan statistic in the United States. Spatial and spatio-temporal epidemiology, 34, 100354.

Hu, Z., Zhang, Y., & Tang, R. (2023). Patterns of Community-Based Data in the US State-Level COVID-19 Dashboards: Groupings, Inconsistencies and Gaps. Proceedings of the Association for Information Science and Technology, 60(1), 983-985.

Janssens, D., Wets, G., Timmermans, H. J. P., & Arentze, T. A. (2007, June). Modeling short-term dynamics in activity-travel patterns: the feathers model. In Innovations in Travel Demand Modeling Conference (pp. 71-77).

Jia, J. S., Lu, X., Yuan, Y., Xu, G., Jia, J., & Christakis, N. A. (2020). Population flow drives spatio-temporal distribution of COVID-19 in China. Nature, 582(7812), 389-394.

Jo, G., Habib, D., Varadaraj, V., Smith, J., Epstein, S., Zhu, J., ... & Swenor, B. K. (2022). COVID-19 vaccine website accessibility dashboard. Disability and Health Journal, 15(3), 101325.

Kan, Z., Kwan, M. P., Wong, M. S., Huang, J., & Liu, D. (2021). Identifying the space-time patterns of COVID-19 risk and their associations with different built environment features in Hong Kong.

Kitamura, R. (1988). An evaluation of activity-based travel analysis. Transportation, 15, 9-34.

Kogan, N. E., Clemente, L., Liautaud, P., Kaashoek, J., Link, N. B., Nguyen, A. T., ... & Santillana, M. (2021). An early warning approach to monitor COVID-19 activity with multiple digital traces in near real time. Science Advances, 7(10), eabd6989.

Kwan, M. P., & Casas, I. (2006). Gabriel: Gis activity-based travel simulator. activity scheduling in the presence of real-time information. GeoInformatica, 10, 469-493.

Labee, P., Rasouli, S., & Liao, F. (2022). The implications of Mobility as a Service for urban emissions. Transportation Research Part D: Transport and Environment, 102, 103128.

Ligmann-Zielinska, A., Siebers, P. O., Magliocca, N., Parker, D. C., Grimm, V., Du, J., ... & Ye, X. (2020). 'One size does not fit all': A roadmap of purpose-driven mixed-method pathways for sensitivity analysis of agent-based models. Journal of Artificial Societies and Social Simulation, 23(1).

Liu, F., Wang, J., Liu, J., Li, Y., Liu, D., Tong, J., ... & Mo, S. (2020). Predicting and analyzing the COVID-19 epidemic in China: Based on SEIRD, LSTM and GWR models. PloS one, 15(8), e0238280.

Mao, L., & Bian, L. (2010). Spatial–temporal transmission of influenza and its health risks in an urbanized area. Computers, environment and urban systems, 34(3), 204-215.

McNally, M. G., & Rindt, C. R. (2007). The activity-based approach. In Handbook of transport modelling (Vol. 1, pp. 55-73). Emerald Group Publishing Limited.

Miller, E. J. (2019). Agent-based activity/travel microsimulation: what's next?. The Practice of Spatial Analysis: Essays in Memory of Professor Pavlos Kanaroglou, 119-150.

Owusu, C., Desjardins, M. R., Baker, K. M., & Delmelle, E. (2019). Residential mobility impacts relative risk estimates of space-time clusters of chlamydia in Kalamazoo County, Michigan. Geospatial health, 14(2).

Rainer, H., & Krause, U. (2002). Opinion dynamics and bounded confidence: models, analysis and simulation.

Rasouli, S., & Timmermans, H. (2014). Activity-based models of travel demand: promises, progress and prospects. International Journal of Urban Sciences, 18(1), 31-60.

Ren, J., Yang, J., Wu, F., Sun, W., Xiao, X., & Xia, J. C. (2023). Regional thermal environment changes: Integration of satellite data and land use/land cover. Iscience, 26(2).

Soleimani, M., & Bagheri, N. (2021). Spatial and temporal analysis of myocardial infarction incidence in Zanjan province, Iran. BMC Public Health, 21(1), 1-14.

Wang, D., & Cheng, T. (2001). A spatio-temporal data model for activity-based transport demand modelling. International Journal of Geographical Information Science, 15(6), 561-585.

Wisconsin Department of Health Services. (2023). COVID-19 Public Use Data. Retrieved August 22. 2023, from https://www.dhs.wisconsin.gov/covid-19/data.htm

World Health Organization. (2024). With the international public health emergency ending, WHO/Europe launches its transition plan for COVID-19. Retrieved January 25, 2024, from. https://www.who.int/europe/news/item/12-06-2023-with-the-international-public-health-emergency-ending--who-europe-launches-its-transition-plan-for-covid-19

Zhou, S., Zhou, S., Zheng, Z., & Lu, J. (2021). Optimizing spatial allocation of COVID-19 vaccine by agent-based spatiotemporal simulations. GeoHealth, 5(6), e2021GH000427.

Appendix

Table 6. Weekday average travels by Age Group

Age Group	Date	# Travels (average dwell time)											
		Work	School	Univ/ College	Daycare	Relig Act	Large Shop	Daily Grocery	Meals	Visit F/R	Recre/ Leisure	Service trips	Others
Child	2020/9	18.2 (363.4)	1023.9 (390.2)		1003.8 (391.2)		436.8 (48.1)	214.7 (48.8)	380.1 (63.0)	464.1 (188.8)	661.4 (135.3)	481.8 (55.6)	285.0 (75.0)
	2020/10	19.7 (365.4)	1019.8 (390.3)		1007.7 (387.7)		398.2 (48.0)	199.2 (48.1)	394.8 (63.9)	452.6 (192.8)	650.2 (135.1)	466.3 (54.7)	287.9 (77.6)
	2020/11	17.6 (357.1)	1000.4 (391.1)		972.8 (391.0)		374.9 (49.4)	190.5 (48.9)	346.9 (63.0)	423.3 (192.2)	596.4 (136.1)	428.3 (56.3)	267.2 (77.4)
	2021/10	18.4 (374.4)	983.0 (392.3)		971.0 (393.6)		389.9 (48.4)	167.1 (51.3)	377.6 (63.5)	521.6 (198.1)	782.1 (135.8)	551.1 (55.3)	285.7 (76.8)
	2021/11	19.0 (368.9)	1045.4 (392.1)		991.7 (390.1)		410.9 (49.4)	182.1 (50.4)	350.7 (65.1)	522.9 (198.7)	767.9 (135.2)	540.0 (55.9)	286.4 (74.9)
	2021/12	19.3 (386.2)	963.9 (392.7)		942.5 (392.7)		359.1 (48.8)	151.8 (51.8)	414.8 (65.1)	507.2 (197.1)	742.2 (138.1)	518.4 (54.2)	282.7 (77.5)
Teen	2020/9	157.6 (342.1)	1719.7 (404.5)				514.4 (47.4)	226.1 (47.7)	467.2 (51.2)	513.2 (190.6)	782.2 (139.5)	528.9 (64.6)	287.0 (190.3)
	2020/10	175.0 (340.7)	1765.4 (404.6)				455.5 (46.9)	206.1 (48.2)	507.1 (50.1)	501.1 (188.4)	764.2 (139.1)	527.8 (65.7)	296.7 (175.4)
	2020/11	163.8 (342.8)	1878.5 (407.9)				425.5 (46.4)	191.3 (51.2)	449.0 (51.6)	462.1 (190.6)	702.8 (138.5)	480.8 (68.7)	265.6 (178.6)
	2021/10	183.3 (348.9)	1872.3 (406.0)				456.6 (47.3)	183.9 (46.0)	468.3 (51.0)	590.1 (194.6)	896.3 (142.5)	615.4 (66.5)	306.9 (183.3)
	2021/11	195.2 (345.2)	1846.3 (406.7)				494.6 (48.3)	198.8 (46.0)	424.3 (51.2)	581.1 (193.2)	905.3 (141.2)	602.8 (66.3)	310.5 (188.0)
	2021/12	182.2 (349.1)	1817.9 (406.7)				423.0 (49.0)	171.0 (48.4)	481.0 (51.0)	553.1 (191.2)	852.7 (140.5)	583.8 (64.9)	301.1 (179.2)
Adult	2020/9	2171.4 (436.3)		805.3 (135.1)	819.7 (134.1)		1315.5 (43.0)	495.3 (41.6)	1025.1 (46.1)	613.3 (170.5)	975.6 (101.0)	914.4 (65.9)	283.9 (183.9)
	2020/10	2214.9 (435.6)		838.5 (135.7)	868.8 (133.3)		1210.2 (42.2)	439.5 (42.0)	1075.7 (45.2)	611.3 (174.0)	961.2 (103.1)	907.0 (66.6)	287.1 (174.9)
	2020/11	2233.7 (443.4)		938.1 (143.2)	976.9 (137.9)		1136.3 (43.4)	411.9 (42.4)	964.0 (45.8)	553.4 (173.5)	877.9 (103.0)	826.4 (75.1)	259.4 (185.7)
	2021/10	2212.8 (445.8)		840.5 (138.6)	877.5 (136.3)		1071.7 (42.5)	405.0 (43.5)	999.2 (46.0)	685.4 (174.4)	1060.9 (103.1)	999.1 (67.9)	308.2 (180.9)
	2021/11	2332.7 (440.7)		854.0 (139.0)	879.8 (136.2)		1102.6 (43.2)	428.8 (42.4)	922.3 (46.7)	672.5 (170.5)	1058.9 (104.1)	994.9 (67.9)	304.8 (183.2)
	2021/12	2340.7 (447.4)		815.3 (140.2)	830.0 (140.9)		1019.1 (42.6)	386.4 (44.0)	912.7 (46.0)	642.9 (176.5)	1019.2 (104.0)	953.2 (69.1)	287.8 (186.9)
Mid-Adult	2020/9	2402.6 (421.0)			940.3 (62.5)	965.5 (62.1)	1678.0 (38.3)	613.4 (38.4)	1200.5 (50.4)	679.3 (160.3)	1031.6 (103.6)	1306.8 (63.3)	443.5 (151.5)
	2020/10	2392.2 (421.3)			933.1 (62.8)	962.6 (63.0)	1608.6 (38.3)	568.1 (38.1)	1163.0 (50.7)	677.6 (162.5)	1030.4 (103.6)	1305.6 (62.5)	444.7 (146.5)
	2020/11	2413.3 (430.6)			935.8 (64.1)	967.4 (65.1)	1480.4 (38.7)	516.5 (38.6)	1044.9 (51.2)	618.5 (165.6)	934.2 (104.6)	1198.5 (65.2)	400.1 (149.8)
	2021/10	2556.8 (433.8)			898.2 (65.6)	923.0 (65.4)	1383.3 (38.7)	551.4 (38.9)	1156.1 (51.7)	822.7 (166.8)	1155.9 (104.8)	1405.2 (65.0)	524.6 (153.9)
	2021/11	2724.2 (429.8)			933.8 (63.1)	973.4 (63.6)	1411.9 (38.9)	574.7 (38.9)	1098.7 (51.5)	812.0 (164.0)	1149.3 (104.2)	1400.5 (64.7)	503.7 (151.6)
	2021/12	2668.3 (436.6)			856.5 (65.2)	892.6 (65.4)	1302.7 (39.0)	508.9 (38.8)	1061.1 (52.2)	764.1 (165.4)	1105.0 (104.6)	1356.7 (65.8)	486.9 (150.2)
Seniors	2020/9	343.8 (342.1)			371.8 (69.1)	408.1 (69.7)	972.6 (40.3)	414.0 (40.2)	556.6 (58.7)	511.2 (134.8)	646.1 (107.6)	939.7 (55.2)	393.8 (134.4)
	2020/10	347.8 (340.5)			406.2 (71.7)	419.7 (70.5)	941.5 (40.9)	377.6 (40.1)	565.0 (58.7)	511.7 (131.4)	640.6 (106.2)	925.7 (55.7)	395.8 (132.4)
	2020/11	344.1 (351.6)			384.1 (71.3)	404.8 (71.9)	796.8 (40.9)	340.3 (41.0)	520.0 (58.7)	470.6 (132.6)	583.2 (107.9)	870.6 (57.2)	366.6 (133.6)
	2021/10	370.7 (353.6)			370.9 (71.8)	379.0 (71.6)	857.7 (41.3)	378.1 (41.9)	582.8 (59.9)	616.0 (133.0)	778.5 (108.0)	1067.1 (57.4)	464.0 (134.8)
	2021/11	397.8 (352.1)			408.2 (70.0)	433.0 (74.2)	914.5 (40.8)	409.3 (41.1)	543.7 (59.3)	617.1 (132.3)	766.3 (107.8)	1063.2 (57.1)	449.2 (133.0)
	2021/12	377.9 (356.6)			350.4 (73.7)	365.5 (72.9)	795.8 (41.5)	348.4 (41.4)	582.8 (59.7)	579.7 (137.3)	725.1 (108.1)	1028.8 (58.6)	431.0 (133.6)

* Relig Act: Religious activity, Visit F/R: visiting friends or relatives
* Grey cell: top 3 trip purpose by month

Table 7. Weekend travels by Age Group

Age Group	Date	# Travels (average dwell time)											
		Work	School	Univ/ College	Daycare	Relig Act	Large Shop	Daily Grocery	Meals	Visit F/R	Recre/ Leisure	Service trips	Others
Child	2020/9	19.4 (97.8)	245.4 (136.4)		226.7 (139.5)	246.5 (133.6)	407.1 (50.1)	191.8 (49.6)	373.2 (51.4)	396.3 (167.4)	505.2 (122.4)	266.5 (55.4)	196.3 (53.7)
	2020/10	20.4 (90.5)	243.8 (136.3)		240.6 (138.3)	269.9 (132.8)	378.6 (50.7)	173.3 (51.0)	372.1 (51.0)	400.4 (169.5)	500.5 (125.6)	285.3 (58.5)	200.4 (55.0)
	2020/11	22.2 (79.4)	280.1 (134.8)		266.0 (132.0)	279.2 (124.7)	408.0 (48.8)	185.6 (48.4)	386.8 (49.6)	427.5 (162.2)	547.5 (121.7)	281.8 (52.2)	210.3 (49.4)
	2021/10	23.7 (80.8)	204.3 (132.1)		211.2 (134.4)	286.4 (124.2)	442.1 (48.3)	190.6 (48.2)	393.2 (49.1)	557.3 (163.7)	670.6 (120.8)	377.4 (51.7)	252.3 (49.3)
	2021/11	19.9 (91.7)	230.4 (140.6)		221.0 (142.5)	261.4 (139.2)	388.3 (51.3)	180.0 (50.4)	348.0 (51.0)	466.0 (167.2)	561.6 (123.8)	309.8 (55.5)	217.1 (52.6)
	2021/12	18.0 (106.1)	181.5 (148.8)		176.5 (144.7)	199.4 (141.2)	321.3 (54.4)	146.2 (53.4)	326.7 (51.4)	401.6 (174.1)	477.6 (122.4)	264.8 (62.1)	174.6 (63.8)
Teen	2020/9	116.0 (324.3)				490.7 (144.7)	424.8 (48.5)	196.5 (47.6)	421.0 (56.2)	445.1 (176.3)	553.0 (149.7)	293.1 (45.6)	230.2 (124.0)
	2020/10	101.0 (326.3)				508.9 (145.8)	470.6 (49.0)	197.3 (49.3)	408.0 (57.4)	453.5 (176.3)	561.7 (150.1)	297.0 (42.5)	237.6 (125.1)
	2020/11	123.3 (308.4)				571.9 (136.0)	506.2 (46.2)	210.2 (46.0)	456.7 (54.6)	470.6 (164.9)	600.2 (146.0)	297.3 (43.2)	233.9 (115.4)
	2021/10	142.5 (310.9)				543.2 (133.8)	508.4 (48.5)	216.2 (49.3)	485.0 (56.1)	630.9 (169.3)	769.4 (146.1)	409.0 (44.3)	303.4 (113.9)
	2021/11	130.6 (322.2)				472.4 (146.6)	446.6 (49.9)	194.3 (50.4)	413.9 (57.7)	525.6 (176.5)	642.5 (150.6)	336.0 (47.8)	253.4 (126.3)
	2021/12	109.9 (335.1)				376.5 (151.6)	397.5 (50.2)	165.3 (51.9)	387.0 (59.6)	441.1 (183.3)	546.6 (152.6)	290.6 (45.9)	217.2 (137.0)
Adult	2020/9	465.0 (327.1)			412.0 (94.3)	366.1 (95.1)	830.3 (42.6)	307.3 (41.9)	802.5 (54.4)	614.2 (174.1)	805.2 (125.7)	442.3 (55.0)	169.6 (177.6)
	2020/10	452.9 (320.1)			425.3 (92.1)	374.2 (93.7)	850.6 (44.3)	303.4 (43.4)	715.7 (54.6)	620.1 (174.2)	821.8 (125.4)	457.1 (55.9)	175.0 (163.2)
	2020/11	522.0 (298.3)			487.1 (88.5)	431.7 (88.0)	1029.9 (41.2)	339.1 (40.6)	937.3 (53.6)	674.8 (166.1)	913.0 (119.8)	487.5 (50.9)	180.5 (155.5)
	2021/10	578.1 (302.2)			444.1 (86.7)	415.5 (90.5)	961.5 (42.4)	360.9 (41.3)	898.9 (52.6)	830.1 (167.7)	1080.3 (121.3)	619.4 (50.6)	232.8 (161.1)
	2021/11	488.7 (321.8)			376.1 (96.6)	350.7 (92.1)	833.3 (43.2)	320.0 (42.7)	742.2 (54.1)	694.9 (176.3)	896.7 (127.8)	513.7 (57.8)	182.5 (176.1)
	2021/12	407.5 (344.7)			294.3 (100.1)	278.4 (101.5)	722.9 (44.8)	268.4 (42.5)	637.0 (54.7)	594.2 (180.2)	775.5 (127.9)	437.7 (59.5)	151.7 (176.2)
Mid-Adult	2020/9	381.1 (282.0)			512.2 (90.5)	530.6 (90.3)	1215.4 (40.6)	400.9 (40.3)	926.9 (55.4)	623.3 (154.2)	816.7 (122.0)	606.5 (43.6)	250.0 (150.1)
	2020/10	376.6 (283.4)			526.8 (90.6)	546.2 (90.2)	1212.7 (41.3)	393.8 (40.3)	821.9 (55.7)	645.2 (155.1)	837.9 (122.2)	621.4 (44.4)	257.6 (147.8)
	2020/11	457.9 (254.6)			626.9 (82.6)	645.6 (83.1)	1361.6 (39.5)	423.6 (39.6)	1036.6 (53.9)	716.2 (143.3)	945.9 (117.4)	682.9 (40.8)	260.2 (133.8)
	2021/10	493.1 (255.2)			563.6 (84.5)	583.4 (84.7)	1406.4 (40.0)	492.3 (39.8)	955.3 (53.7)	863.7 (145.6)	1096.9 (118.1)	838.4 (41.6)	353.8 (134.0)
	2021/11	433.8 (285.1)			517.4 (90.1)	536.2 (90.8)	1168.7 (40.9)	427.7 (40.6)	855.5 (55.4)	719.7 (154.4)	910.4 (123.4)	703.5 (45.8)	288.3 (150.8)
	2021/12	355.0 (302.8)			412.3 (94.1)	435.0 (94.9)	1006.8 (41.1)	352.5 (41.8)	711.0 (56.2)	607.8 (162.4)	770.5 (125.4)	593.0 (48.3)	246.2 (155.6)
Seniors	2020/9	72.6 (232.7)			247.2 (102.6)	265.8 (103.3)	499.4 (38.9)	215.2 (37.3)	355.5 (60.5)	342.4 (135.9)	372.2 (108.5)	339.9 (37.3)	165.6 (114.6)
	2020/10	70.1 (234.9)			266.9 (105.9)	282.1 (104.2)	480.8 (39.2)	200.1 (38.3)	381.8 (59.7)	353.6 (134.5)	378.9 (107.2)	344.5 (36.9)	168.8 (112.9)
	2020/11	86.7 (223.1)			305.6 (98.1)	316.7 (97.1)	543.7 (38.0)	220.6 (36.9)	414.9 (58.3)	362.7 (127.2)	393.1 (103.8)	358.8 (35.3)	170.2 (102.8)
	2021/10	98.0 (229.8)			271.5 (96.9)	283.9 (101.9)	604.7 (37.6)	251.1 (38.4)	430.0 (58.4)	498.9 (130.6)	537.5 (106.5)	494.7 (35.6)	220.4 (105.2)
	2021/11	83.4 (241.4)			259.7 (105.4)	265.3 (104.1)	523.0 (39.3)	228.5 (38.6)	377.7 (60.8)	413.7 (135.9)	447.8 (108.2)	406.7 (36.6)	175.2 (106.5)
	2021/12	72.7 (262.0)			195.8 (110.6)	210.7 (106.5)	410.8 (39.1)	170.7 (39.2)	329.9 (60.6)	349.6 (142.3)	382.6 (111.4)	346.4 (38.2)	152.7 (121.0)

* Relig Act: Religious activity, Visit F/R: visiting friends or relatives
* Grey cell: top 3 trip purpose by month